Int J Adv Manuf Technol (2015) 78:1407–1414
DOI 10.1007/s00170-014-6751-1

ORIGINAL ARTICLE

Researches on physical field evolution of micro-cutting of steel H13 by micron scale ceramic cutter based on finite element modeling

Hongjun Hu · Zhiye Zhai · Yunyang Li · Hao Wang · Junlin Dai

Received: 3 September 2014 / Accepted: 19 December 2014 / Published online: 9 January 2015

Abstract The purpose of this study is to investigate the wear characteristics of ceramic cutter with size 1 μm for ultra micro-cutting of steel H13. The three-dimensional (3D) finite element model of micro-cutting has been developed, and micro-cutting conditions of simulation and material properties have been applied. The simulation results show that cutting forces along *X* and *Z* directions are more stable and smaller than the force along *Y* direction comparatively. And, the force fluctuation increases with rise of cutting speeds. The cutter wears increase with the rise of cutting speeds. There exist minor differences between maximum temperatures in cutter/workpiece during micro-cutting, and the deviation values are about 10 °C. Through these researches, some physical field evolution of micro-cutting parameters could be predicted, and it could be helpful to predict the variation of cutting force, cutter wears, and temperature evolutions. The obtained results could provide the fundamental and practical guidelines for choices of cutting speeds for the metal micro-cutting by ceramic cutter.

Keywords Micron ceramic cutter · Micro-cutting · Wear characteristics · Cutting speed · Cutting force · Cutting temperature

1 Introduction

Miniaturization technologies have great potentials in the industry. Micro-cutting is one of the material fabrication technologies. Micro-cutting technology can meet many of those demands of miniaturized components in fields that include information technology, optics, telecommunication industries, etc. [1]. The normally used micro-cutter types for micro-cutting operations are cutting, end mill, ball nose, drills, and engraving tools. These tools are usually made of tungsten carbide or ceramics.

The basic principles of micro-cutting are similar to conventional cutting, but fundamentally different from macro-cutting in many aspects [2]. Micro-cutting refers to mechanical micro-cutting of removal of materials using geometrically defined cutter edges carried out on micro-machines. Micro-cutting is normally used for machining high-accuracy components in a variety of engineering materials [3]. Main principles of micro-cutting are similar to those of conventional cutting operations; in particular, the surface burrs of the workpiece are removed using micro-cutters. However, unlike conventional macro-cutting processes, micro-cutting displays different characteristics due to its significant minute size. The major differences between micro- and macro-cutting are specific cutting energy, minimum chip thickness, surface roughness, burr, micro-structure effect, and tool wear [4]. One of the main limiting factors for the miniaturization of the cutting process is the tool due to the reduced stiffness of the tiny sizes. Common tool wear in conventional cutting cannot be used as a tool life criterion of ultra micro-cutting.

Mostly used methods for the characterization of micro-cutting include molecular dynamics simulation, finite element method. The underlying theory in the finite element modeling of machining is macro-scale continuum mechanics, and it has been mostly used for investigating orthogonal micro-cutting. Afazov et al. [5] developed mathematical model for determining the uncut chip thickness in micro-cutting successfully which takes into account the run-out effect, angle of rotation, number of flutes, cutting tool radius, feed rate, and spindle

H. Hu (✉) · Z. Zhai · Y. Li · H. Wang · J. Dai
College of Materials Science and Engineering, Chongqing University of Technology, 400050 Chongqing, China
e-mail: hhj@cqut.edu.cn

angular velocity. Chae et al. [6] investigated the current efforts in mechanical micro-cutting research and applications, especially for micro-cutting operations, and suggested that areas from macro-cutting should be examined and researched for application to the improvement of micro-cutting processes. Tansel et al. [7] studied the relationship between the cutting force characteristics and tool usage (wear) in a micro-end-cutting operation for two different metals. Cui et al. [8] revealed the failure mechanisms of Al_2O_3-(W, Ti)C ceramic tools in intermittent cutting of hardened AISI 1045 steel by means of damage mechanics, and a damage model has been constructed by means of micro-mechanics in order to investigate the representative volume element subjected to tri-axial stress induced by the mechanical and thermal loads. Afazov [9] proposed an advanced micro-cutting force model considering the tool wear, and the micro-cutting forces have been predicted and compared with experimentally obtained results for two cutting conditions and four edge radii measured at different stages of the tool wear.

Introduced in the early 1950s, fine-grained high-purity aluminum oxide (Al_2O_3) is pressed into insert tip shapes and sintered at high temperatures. Although FEM methods of the micro-cutting process have been researched in many papers, there was hardly a FEM research on the micron dimension cutter made of Al_2O_3 ceramics, and idealized models and boundary conditions for micro-cutting process are inadequate. Micron dimension cutter as a novel tool with its unique high-temperature performance is used in micro-cutting process; its thermal characteristics and turning load and wear evolution play an important role in its performance and service life.

In this paper, numerical models of micron Al_2O_3 ceramic cutter and workpiece have been implemented by using commercial finite element software DEFORM™-3D to predict micro-cutting forces, temperatures, and tool wears. Properties of cutter and workpiece have been chosen. Micro-cutting parameters for simulations have been set up. FEM research results have provided essential information about the mechanics of micro-cutting by Al_2O_3 micron-size ceramic cutter. Curves of cutting forces, temperature prediction, and tool wears have been obtained. Influences of cutting speeds on cutting forces and cutter wears have been explored.

2 Simulation conditions

The three-dimensional (3D) FEM of micro-cutting has been created in the DEFORM-3D v6.1 [10]. FEM of cutter/workpiece for the simulations, after micro-cutting with cutting time 4.49 ms, has been shown in Fig. 1.

The workpiece material for micro-turning is hard steel H13. The hard steel is H13 which is used in high-strength mechanical components for automotive and aerospace industry [11]. H13 has good thermal shock resistance and high hardenability, excellent wear resistance, and hot toughness and will tolerate some water cooling in service. The properties of single-grain ceramic tool are as follows: the density is 3500 kg/m^3, the Young's modulus is 415 GPa, the Poisson's ratio is 0.22, the thermal expansion is 8.4e−06, the specific heat is 334 J/kg K, and the thermal conductivity is 7.5 W/m K.

The micro-cutting conditions with size 1-μm cube cutter for FEM simulation have been presented in Table 1. The basic assumptions involved in the study are as follows: the generated heat flow and the temperature distribution are in steady state, and all of the deformation energy has been converted into heat. Heat loss along the interface and at all surfaces of the tool and the chip is ignored. The dimensions of the tool are larger than the chip cross section. The primary and the secondary heat sources are plane heat sources, and the nature of

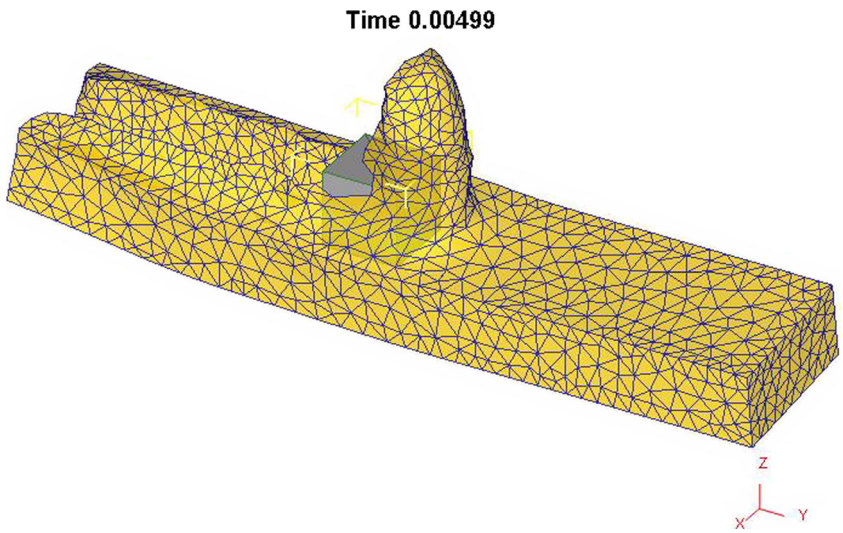

Fig. 1 Finite element model of cutter workpiece for the simulations after micro-cutting with cutting time 4.49 ms

Table 1 Micro-cutting parameters for simulations

Workpiece material	H13 steel
Cutter material	Micron ceramics
Cutting speed (mm/s)	0.1, 1, 2
Depth of cut (μm)	0.5
The initial cutting temperature and the initial environmental temperature (°C)	20
Shear friction coefficient between the cutter and chip interface	0.7
Width of cut (μm)	1
Max element size of cutter	0.22 μm
Min element size of cutter	0.11 μm
Cutter mesh size ratio	2
Element numbers of cutter	1403
Workpiece type	Plastic
Heat transfer coefficient (N/s/mm/C)	11
Maximum number of nodes for workpiece	2744
Number of elements for workpiece	11,183

the secondary heat source is not affected by the possible crater wear.

Cutting speed (also called surface speed or simply speed) could be defined as the speeds that the material moves past the cutting edge of the tool, irrespective of the machining operation used. Cutting speeds are 0.1, 1, and 2 mm/s, respectively, in the simulations. In Table 1, the initial cutting temperature and the initial environmental temperature and shear friction coefficient between the cutter/chip interfaces are initial and boundary conditions. The material is attached to the mesh, with periodic remeshing to avoid severe element distortion. Automatic and adaptive remeshing was used to take into account the severe distortion of mesh elements near the tool tip, so very fine meshes were used near the tool tip in the

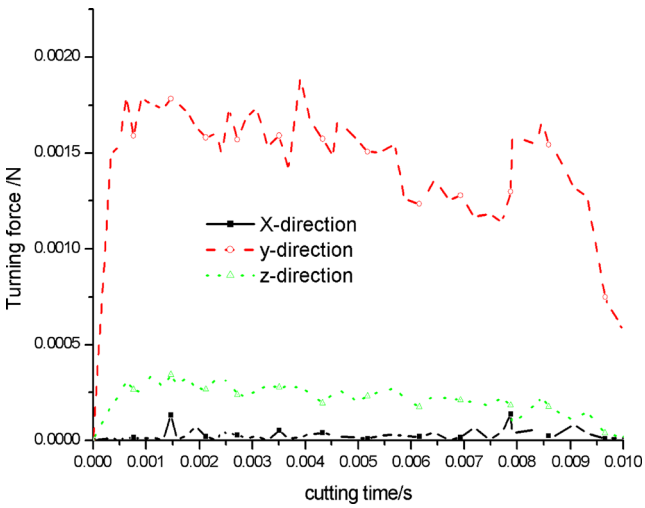

Fig. 2 Curves of micro-cutting force for *X*, *Y*, and *Z* directions with cutting speed 1 mm/s

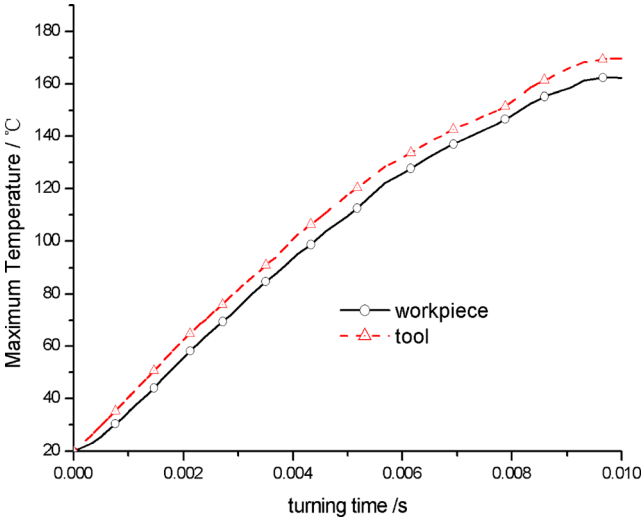

Fig. 3 Simulation maximum temperature for cutter and workpiece vs. time with the cutting speed of 1 mm/s

deformation zone of the workpiece and the edge of the 3D model tool for micro-turnings based on micro-scale. The number of surface elements represents the approximate number of surface elements that will be generated by the mesh generator.

3 Results and discussions

3.1 Curves of cutting forces during micro-cutting

Cutting forces play an important role in the micro-cutting process [11], which is a process of extensive stresses and plastic deformations. Cutting force is a force that is generated by the cutting tool as it machines the workpiece. The high compressive and frictional contact stresses on the tool face would result in a substantial cutting force. For many researchers it is calculated just in the steady condition by empirical formulas, and which make it impossible to observe the force variation.

In micro-cutting, the total cutting force is conveniently resolved into three components. The resultant force Fr is transmitted across the chip-tool interface. Components on shear plane are Fs in the plane and Ns normal to shear plane. Cutting force Fp is in the cutting direction and a trust force Fq normal to the workpiece surface. On the rake face, the friction force Fc is in direction of chip flow and the normal force Nc is normal to the rake face. Through the general postprocessor and the time-history postprocessor in the FEM DEFORM software, the calculated results can be displayed. Users can obtain cutting forces between tool/chip from simulation results.

Figure 2 presents the variation of the simulated cutting forces of the three directions *X*, *Y*, and *Z*, which have been obtained from numerical simulation with a very narrow range

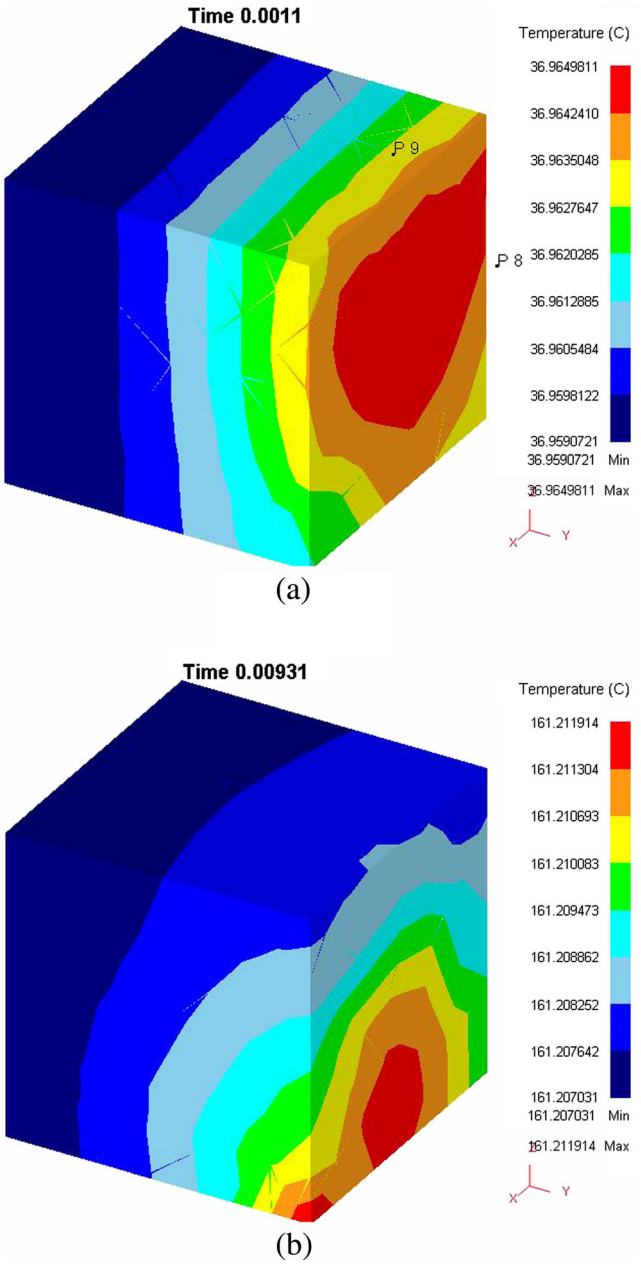

Fig. 4 The isothermal ribbons of cutter during micro-cutting with cutting speed 1 mm/s: **a** 0.0011 s and **b** 0.00931 s

time 0.01 s. The curves show that cutting forces of the three directions are fluctuations. At the beginning of cutting, the cutting force rises sharply for Y direction and the other two forces increase gradually until the cutting time is about 0.5 ms. But, to the forces of X and Z directions, the cutting forces are steadier than the force of Y direction comparatively. Curves show that the predicted maximum cutting forces of three principal directions X, Y, and Z are 0.2, 20, and 0.4 mN, respectively. The Y direction force is the biggest among the three micro-cutting forces, which would overcome resistance of metal along the cutting direction. And, the Y direction force is the primary cutting force which is directly generated by the relative motion of the cutting tool with respect to the workpiece during cutting, and it occurs in the same direction as cutting tool movement. Cutting forces of the three directions are fluctuations for the influences of cutter temperatures on the resistances of metal. At the beginning of machining, the cutting force rises sharply for Y direction and the other two forces increase gradually. For the forces of X and Z directions, the cutting force is steadier than that for the forces of Y direction comparatively. And, the force fluctuations increase with the rise of cutting speeds.

3.2 Temperature prediction for micro-cutting process

Several analytical methods such as calorimetric method, and moved thermocouple technique and embedded thermocouple technique to calculate cutting temperature derived from dimensional analysis by using experimental data for various work materials [11].

$$T = \frac{0.4U}{\rho C}\left(\frac{vt_0}{K}\right)0.333 \tag{1}$$

where T is the temperature rise at cutter/chip interface, U is the specific energy and cutting speed, t_0 is the chip thickness before cut, C is the volumetric specific heat of work material, and K is the thermal diffusivity of the work material.

The speed and temperature relationship is determined to be of the form Eq. (2) [3].

$$T = Kv^m \tag{2}$$

where T is the measured tool/chip interface temperature. The maximum temperature curves for cutter and workpiece are shown in Fig. 3. It is established based on temperature changes with micro-cutting that the time required to reach the steady-state temperature is 0.01 s.

It can be seen from the curves that the minimum value of the temperature for tool is about 20 °C and the maximum 170 °C. But the maximum temperature of workpiece is about 160 °C. The temperatures of workpiece and cutter increase rapidly. It is suggested that there exist minor differences between maximum temperatures in tool/workpiece during micro-cutting, and the deviations values are about 10 °C [12–15].

Figure 4a shows the isothermal ribbons of cutting temperatures in the cutter with the cutting time of 1.1 ms. Maximum temperatures of the cutter located at the center of initial contact

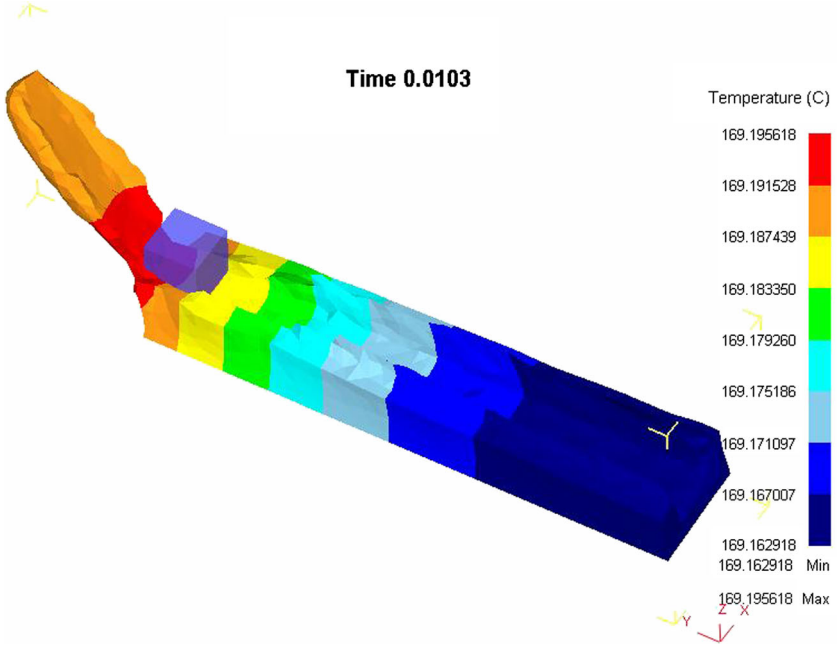

Fig. 5 The temperature distributions of cutter and workpiece at cutting time 0.0103 s

surface with temperatures of the workpiece between 36.9642 and 36.9649 °C. It is clear that the temperature distribution is not uniform and the temperatures of the center in the surface of cutter are highest. The temperature increases rapidly in Fig. 4b, and the highest temperature moves the blade of cutter, for a large amount of friction heat and metal cutting has been generated in the blade.

From Fig. 4, it is clear that the highest temperature center is displacing. The heat generated is emanated by the chip, the cutting tool, and the workpiece [16–19]. That maximum amount of heat is carried away by the chip. From 10 to 20 % of the total heat goes into the tool, and some heat is absorbed in the workpiece. With the increase in cutting speeds, the chip shares heat increasingly.

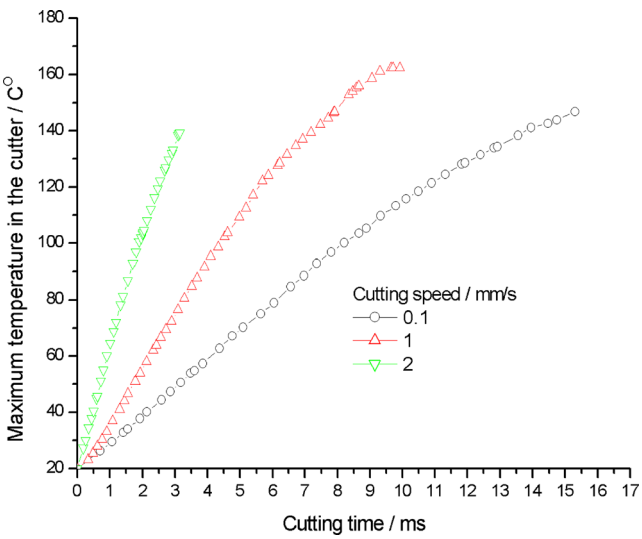

Fig. 6 Maximum temperature vs. time for tool and workpiece in simulation results with different turning speeds

Figure 5 shows the temperature contours for workpiece with cutting time 0.0103 s. The chip is formed with disintegration shapes. The temperatures of the shear zone are about 169.2 °C, and the second highest temperature region is the contact face between the cutter and the workpiece and also the zone of contact between chip/cutter [20, 21]. The temperatures of most nodes in the tool/chip interface are steady at cutting time 0.1 s, and the maximum temperature of base metal is about 169.2 °C which is far away from the melting point. So the surface integrity could not be broken.

The temperature rises during the turning are due to generated shear and frictional heat [2]. It was investigated the effects of turning speeds on maximum temperatures in cutter shown in Fig. 6. The times required to reach the steady-state temperature are 3, 11, and 16 ms for the cutting speed of 0.1, 1, and 2 mm/s, respectively. As can be seen from the curves, the increment speeds of maximum temperatures (140, 165, and 150 °C) for tool increase with turning speed increasing. The simulation results are coordinated with the theoretical calculation formulas (1) and (2). The curves for temperature climb sharply at the beginning until the steady-state approach.

3.3 Tool wears during micro-cutting

Metal cutting tools are subjected to extremely arduous conditions, high loads, and high surface temperatures rise because the chip slides along the tool face while exerting very

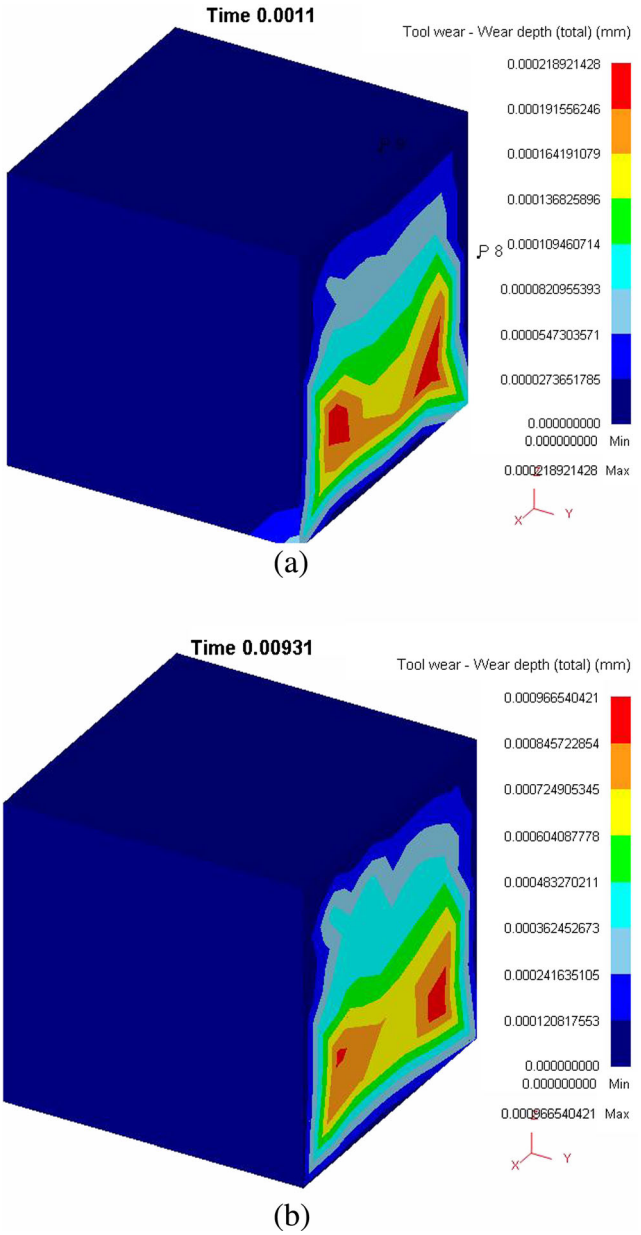

Fig. 7 The isothermal ribbons of cutter during micro-cutting at cutting time of **a** 1.1 ms and **b** 9.31 ms

high normal pressures and friction force on this face. In the early stage of cutting, there is a small area of the sporadic wear on cutter surface only, which are shown in Fig. 7a, and the maximum wear depth at this time is about 0.2189 μm. As the cutting continue, wear area increases gradually. After the cutting time of 0.00931 s, the wear depth exceeds 0.967 μm for the cutter. After the step time of 0.037 s, the estimated accumulative wear depth arrives at 1.1 μm. As can be seen from Fig. 7, the tool wear begins at the center of tool face which contacts the workpiece, and with the cutting development, the wears spread at the center around the center. When the wear area increases to a certain extent, wear zones will no longer be changed too much. The maximum temperatures in the cutter are higher than those in the workpiece.

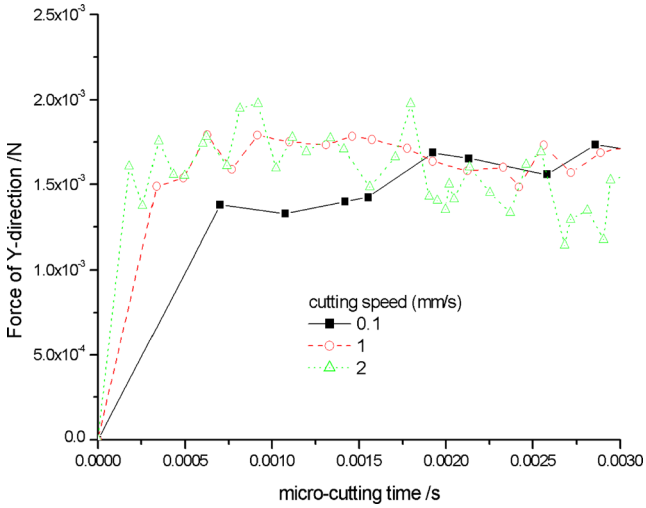

Fig. 8 Curves of cutting forces in *Y* directions for cutting speeds 0.1, 1, and 2 mm/s

3.4 Influences of cutting speeds on cutting forces

Figure 8 presents the variation of the simulated cutting forces of the *Y* direction which has been obtained from numerical simulation of cutting speeds 0.1, 1, and 2 mm/s, respectively, and in a very narrow range time 0.01 s. The curves show that cutting forces of the *Y* directions are fluctuating. The cutting force surges up from 0 to 1.5e −3 N in the short time of about 0.1e−4 s. The abrupt increase of the cutting force on a cutter may cause the damage in the cutter or unexpected wear. The forces are fluctuating due to the presence of hard particles in the component micro-structure or, more extremely, when interrupted cutting is being carried out.

At the beginning of the machining, the cutting force rises rapidly until the cutting time is about 0.001 s. But, the *Y* direction forces are stabilized comparatively after 0.001 s. The reason of the turning force droping is due to that the workpiece metal softens for temperature rise. It is clear that the cutting forces of *Y* direction increase with the rise of cutting speeds. And the force fluctuations increase with the cutting speed rising. Fluctuation range is very wide for cutting speed 2 mm/s. The temperature rise caused by cutting speed 0.1 mm/s is lower than that caused by other speeds.

3.5 Influences of cutting speeds on tool wear

Mathematically, the tool life can be expressed in Taylor Eq. (3).

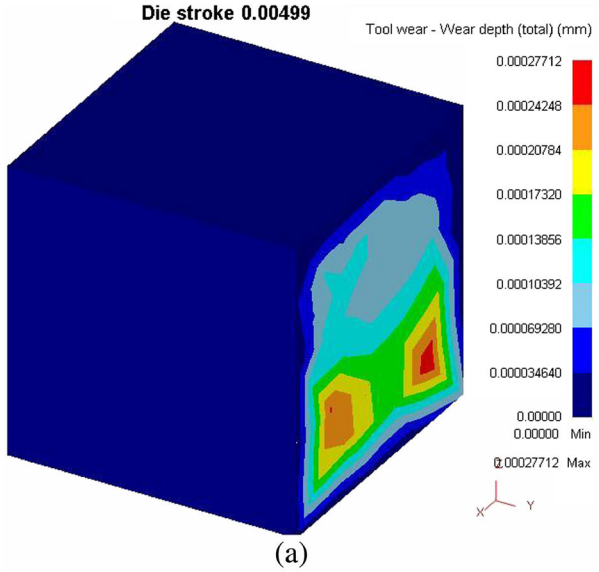

(a)

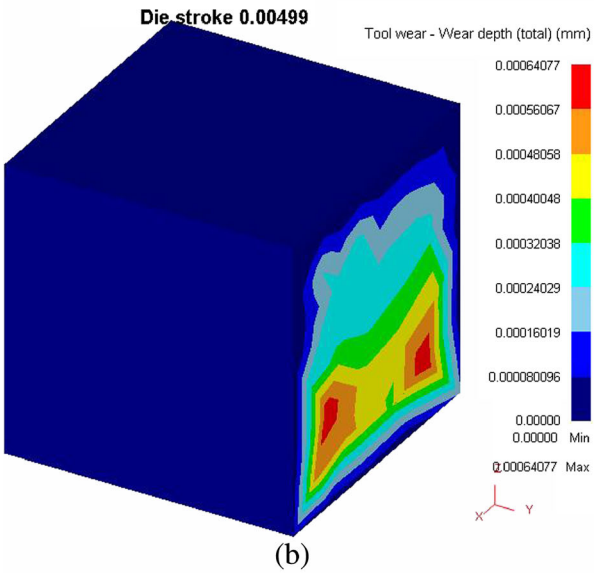

(b)

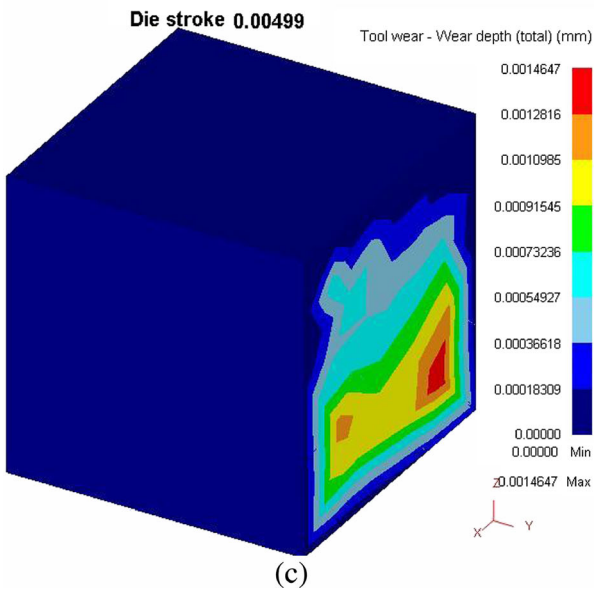

(c)

◀ **Fig. 9** Wear depth evolution with different ceramic cutters at cutting length 0.005 mm with different cutting speeds: **a** 0.1 mm/s, **b** 1 mm/s, and **c** 2 mm/s

$$v\,T^n = C \tag{3}$$

where v is the cutting speed, T is the tool life, C is the cutting speed for a tool life of 1 min, and n is the Taylor exponents which are found by experimentation or published data; they are properties of tool material, workpiece, and feed rate. Among these parameters, the cutting speed is the most critical. As cutting speed is increased, the wear rate increases, so the same wear criterion is reached in less time, i.e., tool life decreases with cutting speed.

The Archard wear equation shown in Eq. (4) is a simple model used to describe sliding wear and is based around the theory of asperity contact.

$$W = \int K\frac{p^a v^b}{H^c}dt \tag{4}$$

where W is the flank wear land width; p is stranded for normal stress between tool flank face and workpiece; v is the sliding velocity; H is the hardness of the cutting tool material; dt is the time increment; and a, b, and c are experimentally calibrated coefficients and equal to 1 and 1 and 2, respectively, in this research.

The simulation results for the cutting length of 0.005 mm can be seen in Fig. 9. It is shown that the dominant wear pattern is crater wear. The tool wear begins with the center of cutter, there exist two wear concentration positions in the contact surface, and the cutting wear spreads around the two centers. Significant differences of cutting wear area are affected by cutting speeds. The maximum wear depth is 0.28 μm which is shown in Fig. 9a. But, the maximum wear depth shown in Fig. 9b increases to 0.64 μm when the cutting speed is 1 m/s. When the cutting speed is 2 m/s, the maximum wear depth is 1.4 μm, as can be seen in Fig. 9c. It is obvious that the cutter wears increase with rise of cutting speeds. In Fig. 9, crater wears are normally the dominating wear mode. At higher cutting speed, the crater formation is inevitable. It is related to the very high temperatures on the tool wear. The most important factors that contribute to crater wear are the cutter/workpiece interface temperature, sliding velocity, and interface pressure between the cutter and workpiece.

4 Conclusion

The 3D FEM of micro-cutting has been created, and micro-cutting conditions of simulation and material properties have

been chosen. The conclusions could be summarized as follows:

1. The cutting forces along *X* and *Z* directions are steadier than the forces along *Y* direction.
2. There exist minor differences between maximum temperatures in tool and workpiece during micro-cutting, and the deviations are about 10 °C. It is clear that the temperature distribution is uniform and the temperatures of cutter surface center are the highest. The maximum temperatures of base metals are far away from the melting point. So, the surface integrity could not be broken. When the wear area increases to a certain extent, wear zone can no longer be changed too much. Maximum temperatures in the cutter are higher than those in the workpiece.
3. The earlier steady state arrives during cutting stage with larger cutting speeds. Cutter wears increase with rises of cutting speeds. The effects of turning speed on the temperature distribution have been researched. The maximum temperatures of workpiece increase with the rise of turning speeds. But, the temperatures of workpiece and tool may remain stable when stable cutting stage reached. The production and dissemination of turning heats are described.

Acknowledgments This work was supported by foundation of the post doctorate in Chongqing city and Project Number Xm201327, China Postdoctoral Science Foundation-funded project 2014 M552575.

References

1. Liu CR, Guo YB (2000) Finite element analysis of the effect of sequential cuts and tool chip friction on residual stresses in a machined layer. Int J Mech Sci 42:1069–1086
2. Qin F, Gong X, Chou K (2011) Size effects in cutting with a diamond-coated tool, Proceedings of the ASME 2011 International Manufacturing Science and Engineering Conference, Corvallis, OR, 267–273
3. Hu HJ, Huang WJ (2013) Studies on wears of ultrafine-grained ceramic tool and common ceramic tool during hard turning using Archard wear model. Int J Adv Manuf Technol 69:31–39
4. Hu HJ, Huang WJ, Wu GS (2013) 3D finite element modeling and experimental researches on turning steel AISI1013 by nano-crystalline Al2O3 ceramics cutter. Int J Mach Mach Mater 14:295–310
5. Afazov SM, Ratchev SM, Segal J (2010) Modeling and simulation of micro-milling cutting forces. J Mater Process Technol 210:2154–2162
6. Chae J, Park SS, Freiheit T (2006) Investigation of micro-cutting operations. Int J Mach Tools Manuf 46:313–332
7. Tansel IN, Arkan TT, Bao WY, Mahendrakar N, Shisler B, Smith D, McCool M (2000) Tool wear estimation in micro-machining. Part I: tool usage–cutting force relationship. Int J Mach Tools Manuf 40: 599–608
8. Cui X, Zhao J, Zhou Y, Zheng G (2013) Damage mechanics analysis of failure mechanisms for ceramic cutting tools in intermittent turning. Eur J Mech A/Solids 37:139–149
9. Afazov SM, Zdebski D, Ratchev SM, Segal J, Liu S (2013) Effects of micro-milling conditions on the cutting forces and process stability. J Mater Process Technol 213:671–684
10. Hu HJ, Huang WJ (2013) Effects of turning speed on high-speed turning by ultrafine-grained ceramic tool based on 3D finite element method and experiments. Int J Adv Manuf Technol 67:907–915
11. Liu W, Liu S, Ma J, Kovacevic R (2014) Real-time monitoring of the laser hot-wire welding process. Opt Laser Technol 57:66–76
12. Liu W, Ma J, Yang G, Kovacevic R (2014) Hybrid laser-arc welding of advanced high-strength steel. J Mater Process Technol 214:2823–2833
13. Kong F, Liu W, Ma J, Levert E, Kovacevic R (2013) Feasibility study of laser welding assisted by filler wire for narrow-gap butt-jointed plates of high-strength steel. Weld World 57:693–699
14. Afazov SM, Ratchev SM, Segal J (2012) Prediction and experimental validation of micro-milling cutting forces of AISI H13 steel at hardness between 35 and 60 HRC. Int J Adv Manuf Technol 62:887–899
15. Aliakbari E, Baseri H (2012) Optimization of machining parameters in rotary EDM process by using the Taguchi method. Int J Adv Manuf Technol 62:1041–1053
16. Tang ZT, Liu ZQ, Pan YZ, Wan Y, Ai X (2009) The influence of tool flank wear on residual stresses induced by milling aluminum alloy. J Mater Process Technol 209:4502–4508
17. Sun H, Wan N, Chang Z, Mo R (2011) Approach to optimization of part machining service combination. Int J Adv Manuf Technol 56: 767–776
18. Wang M, Wang J (2012) CHMM for tool condition monitoring and remaining useful life prediction. Int J Adv Manuf Technol 59:463–471
19. Shao F, Liu Z, Wan Y, Shi Z (2010) Finite element simulation of machining of Ti-6Al-4V alloy with thermodynamically constitutive equation. Int J Adv Manuf Technol 49:431–439
20. Wu ZG, Song M, He YH (2009) Effects of Er on the microstructure and mechanical properties of an as-extruded Al–Mg alloy. Mater Sci Eng A 504:183–187
21. Song M, Wu Z, He Y (2008) Effects of Yb on the mechanical properties and microstructures of an Al–Mg alloy. Mater Sci Eng A 497:519–523